[AMERICAN JOURNAL OF SCIENCE, VOL. 264, JANUARY 1966, P. 37-65]

SYNTHESIS AND STABILITY RELATIONS OF FERROTREMOLITE

W. G. ERNST

Department of Geology and Institute of Geophysics and Planetary Physics, University of California, Los Angeles, California

ABSTRACT. Phase relations were determined for the bulk composition $2CaO \cdot 5FeO_x \cdot 8SiO_2 + H_2O$ at moderate temperatures and fluid (total) pressures, and over a range of oxygen, hydrogen, and H_2O fugacities. The mean index of refraction for synthetic ferrotremolite, $\square Ca_2Fe_5^{++}Si_8O_{22}(OH)_2$, is 1.689 ± 0.003. Average unit cell dimensions are: $a = 9.97 \pm 0.01$ Å; $b = 18.34 \pm 0.02$ Å; $c = 5.30 \pm 0.01$ Å; and $\beta = 104.5 \pm 0.1°$.

With f_{O_2} defined by the magnetite-iron buffer, ferrotremolite is stable up to 437°C at 500 bars P_{fluid}, 543°C at 3000 bars P_{fluid}; the high-temperature assemblage of equivalent composition consists of the phases fayalite + quartz + hedenbergitic pyroxene + fluid. With f_{O_2} specified by the magnetite + quartz-fayalite buffer, the amphibole high-temperature stability limit is reduced about 4°C, and magnetite accompanies the other high-temperature phases. The dehydration reactions evolve about 7.2 ± 5 and 7.5 ± 5 kcal/mole ferrotremolite respectively.

At slightly higher relative oxygen fugacity ranges, ferrotremolite is not stable at any temperature; this bulk composition is represented by a low-temperature assemblage consisting of the phases magnetite + hedenbergitic pyroxene + nontronite (± fluid) where oxygen fugacity is controlled by the bunsenite-nickel buffer and by the assemblage andradite + hematite + magnetite + nontronite (± fluid) where f_{O_2} is controlled by the hematite-magnetite buffer. Above about 420 to 440°C at 3000 bars fluid pressure, the clay mineral decomposes and quartz joins the high-temperature phase assemblages.

Restriction of ferrotremolite in nature stems from three effects. (1) Pure $\square Ca_2Fe_5^{++}Si_8O_{22}(OH)_2$ has a very limited thermal range compared to most other hydrous silicates; low values of the fugacity of H_2O at high lithostatic pressures would further reduce the P-T stability field of the amphibole. (2) Ferrotremolite is stable exclusively at low f_{O_2} so relatively high oxygen fugacities typical of many low-grade metamorphic rocks would favor production of more oxidized mineral assemblages at the expense of ferrotremolite. (3) Rock bulk compositions represent a strong departure from that of $\square Ca_2Fe_5^{++}Si_8O_{22}(OH)_2$; at suitably low temperatures and oxygen fugacities, multiphase equilibria would be expected to enrich the amphibole in magnesium with respect to ferrous iron.

INTRODUCTION AND ACKNOWLEDGMENTS

Warren (1929) determined the crystal structure of tremolite and demonstrated its applicability to other amphiboles (Warren, 1930). The general formula may be written as $A_{0\text{-}1}{}^{X\text{-}XII}X_2{}^{VI\text{-}VIII}Y_5{}^{VI}Z_8{}^{IV}O_{22}(OH)_2$, where Roman superscripts refer to cation coordination. The wide range in sizes of cations which can be accommodated, as reflected by coordination numbers, is explained in terms of the structure and accounts for the great compositional diversity of amphiboles. Based on cation occupancy of the X structural sites, amphiboles generally are classified in terms of three groups, the calcic amphiboles, the alkali amphiboles, and the anthophyllite-grunerites. Calcic amphiboles clearly constitute the most important subdivision, both with regard to total abundance and in the number of distinct species.

Kunitz (1930), Berman (1937), Hallimond (1943), Sundius (1946), Winchell and Winchell (1951), Boyd (1959), Deer, Howie, and Zussman (1963), and Leake (1965) among others have considered chemical variation

among the calcic amphiboles. Although other variants are possible, in general lower grade metamorphic rocks and some scarns carry tremolite-actinolites, $\square Ca_2(Mg,Fe^{++})_5Si_8O_{22}(OH)_2$, subsilicic and iron-rich igneous rocks contain primary pargasites, magnesiohastingsites, or iron-bearing equivalents, $NaCa_2(Mg,Fe^{++})_4(Fe^{+++},Al)Si_6Al_2O_{22}(OH)_2$, and higher grade metamorphic rocks and intermediate igneous rocks carry common blue-green hornblendes, of approximate composition $Na_{0.5}Ca_2(Mg,Fe^{++})_{4.5}(Fe^{+++},Al)_{0.5}Si_7AlO_{22}(OH)_2$ ($\square$ represents nonoccupancy of the A structural site).

Paragenetic relations among calcic amphiboles and other ferromagnesian silicates appear to be exceedingly complicated and are only imperfectly understood at present. Experimental phase equilibrium investigation of the major end members is a necessary step in elucidating these paragenetic relations, for one must proceed from the relatively simple synthetics toward the more complex natural minerals. Thus far the stability relations of tremolite, $\square Ca_2Mg_5Si_8O_{22}(OH)_2$, and paragasite, $NaCa_2Mg_4AlSi_6Al_2O_{22}(OH)_2$, have been published by Boyd (1959); in addition, Gilbert (1965) has determined phase equilibria involving ferropargasite, $NaCa_2Fe_4^{++}AlSi_6Al_2O_{22}(OH)_2$. The present study concerns stability relations of ferrotremolite, $\square Ca_2Fe_5^{++}Si_8O_{22}(OH)_2$. Taken in conjunction with the investigations of Boyd and Gilbert, the present report represents equilibrium data for the fourth synthetic end member of a fundamental compositional quadrilateral; this system, tremolite-ferrotremolite-pargasite-ferropargasite, encompasses many common hornblendes of igneous and metamorphic rocks, as shown in figure 1. In this diagram, octahedral substitution of ferrous iron (+ Mn) for magnesium is shown along the abscissa; along the ordinate, the replacement involves $Na(+K)^{X\text{-}XII}Al^{VI}Al_2^{IV}$ for $\square(Mg.Fe^{++})^{VI}Si_2$. Only those amphiboles that contain $Fe^{+++} < 0.30$, Ti and $K < 0.25$, and $Mn < 0.50$ per 24 anions are plotted in figure 1; calcium ranges from about 1.7 to 2.0, silicon from 6.1 to 8.0 on the same basis, and the Na/Al^{IV} ratio closely approaches 0.5. Chemical variation among natural amphiboles closely approaching the composition $Na_{0\text{-}1}Ca_2(Mg,Fe^{++})_{4\text{-}5}(Fe^{+++},Al)_{0\text{-}1}Si_{6\text{-}8}Al_{0\text{-}2}O_{22}(OH)_2$ appears to range from tremolite to pargasite and well into ferrous iron-bearing analogues: natural occurrences of end member ferropargasite and ferrotremolite have not been reported, except for a manganiferous ferrotremolite (Shannon, 1921). Nevertheless, elucidation of the phase relations for the ferrous as well as magnesian end members, and eventually of the binary solid solutions, is requisite to an understanding of more complex equilibrium relations and parageneses of natural members of this system.

The investigation of ferrotremolite was carried out using facilities of the Department of Geology and Institute of Geophysics and Planetary Physics, University of California, Los Angeles, and was supported in part by a National Science Foundation research grant, no. GP-712. This manuscript has been critically reviewed and materially improved by H. P. Eugster, The Johns Hopkins University, and F. R. Boyd, The Geophysical Laboratory. The author expresses his appreciation to the institutions and individuals named above for their support and advice.

EXPERIMENTAL METHODS

Conventional hydrothermal equipment and techniques were employed in this investigation. Cold seal pressure vessels (Tuttle, 1949) were fabricated from 310 stainless steel and Udimet 500 alloy. Fluid pressure (= total pressure) was applied through a system consisting of an oil pump, an oil-water separator-intensifier, and three large volume high pressure water reservoir tanks; pressure was monitored by a variety of gauges calibrated against a 4000 bar 14 inch Heise bourdon tube gauge taken as standard. Hydrostatic pressure was maintained in individual pressure vessels at values of 500 to 3000 bars for periods up to six months with fluctuations less than ± 20 bars.

Pressure vessels were heated in horizontal nichrome-wound resistance furnaces. Pyrovane regulators and Powerstats supplied with regulated current controlled furnace power. Chromel-alumel thermocouples, placed in external thermocouple wells in the pressure vessels and positioned 13 or 28 mm from the charge capsule, were connected to a stripchart recorder and to a Leeds and Northrup K-3 potentiometer; each furnace + "bomb" was calibrated against the melting point of NaCl (800.5°C) or LiCl (605°C) or was

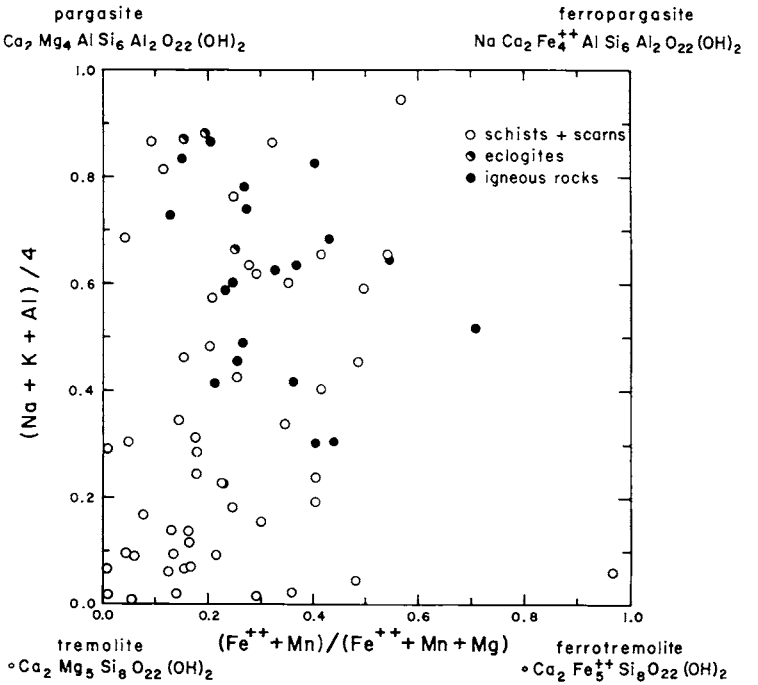

Fig. 1. Compositions of natural amphiboles closely approaching tremolite-ferrotremolite-pargasite-ferropargasite solid solutions. Based on 24 anions, Ca ranges from 1.7 to 2.0, Fe+++ < 0.30, Ti and K < 0.25, and Mn < 0.50 (all samples have Mn < 0.25 except for the specimen that plots nearest the $Ca_2Fe_5{}^{++}Si_8O_{22}(OH)_2$ end member).

plumbed with internal versus external thermocouples. In all cases the external thermocouple in the thermocouple well recorded values within one Celsius degree of the calibrated temperature of the charge. Individual experiments were maintained with temperature fluctuations seldom greater than ± 2C°.

Ferrotremolite contains iron, an element of variable oxidation state, hence oxygen fugacity is a variable that influences phase relations. Accordingly, f_{O_2} was controlled using the buffer technique devised by Eugster (1957). An inner sealed silver-palladium alloy, $Ag_{70}Pd_{30}$, or platinum capsule (outer diameter 3.0 mm) containing the charge + excess H_2O was placed in an outer sealed gold capsule (outer diameter 5.6 mm) containing

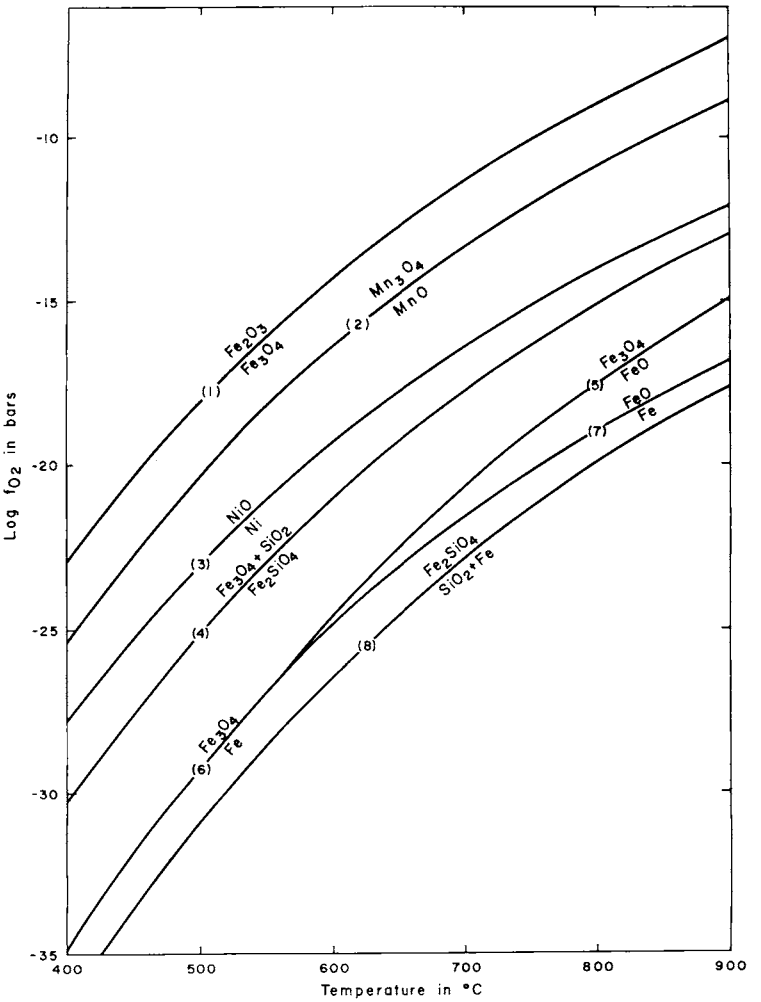

Fig. 2. Log f_{O_2}-T plot of oxygen buffers; the effect of total pressure is negligible. Data are from Eugster and Wones (1962) and Hahn and Muan (1960).

a suitable buffer + excess H_2O. Oxygen, with its fugacity defined by the buffer at fixed temperature and pressure, equilibrated with hydrogen and H_2O in the outer capsule; because the silver-palladium alloy and platinum are permeable to H_2, equilibration with the inner capsule was effected, thus defining the oxygen fugacity of the charge. Silver-palladium alloy run capsules were used for all experiments except those conducted employing the bunsenite-nickel buffer. On these latter runs, because the Ag-Pd capsule reacted with the buffer, platinum capsules were used. An f_{O_2}-T plot of several iron (± silica), nickel, and mangansese oxide buffers is presented in figure 2; locations of curves (1) and (3) to (8) are from the compilation by Eugster and Wones (1962), location of curve (2) is extrapolated from the data of Hahn and Muan (1960). The effect of variation in total pressure on f_{O_2} for a specific buffer at fixed temperature is minor and is well within limits of error for curve location, as discussed previously (Ernst, 1960, p. 15; Eugster and Wones, 1962, p. 91-92).

The condensed charge was made up as a mixture of reagent grade CaO, Fe_2O_3, and SiO_2 in the stochiometric cation proportions of ferrotremolite. The hematite was reduced subsequently to metallic iron by passing hydrogen gas over the oxide mixture at 600°C for approximately one half hour. The resultant material was relatively reactive and after addition of excess distilled H_2O could be converted partly to very fine-grained ferrotremolite at moderate temperatures and fluid pressures; the remainder of the condensed run products consisted of appropriate proportions of the anhydrous phases characteristic of the high-temperature and/or high-oxygen fugacity assemblage equivalent in bulk Ca-Fe-Si proportions to ferrotremolite. The investigated bulk composition was thus $2CaO \cdot 5FeO_x \cdot 8SiO_2 + H_2O$, where x ranged from 1.0 to almost 1.5 (as a function of relative oxygen fugacity range).

All phase descriptions and equilibrium data for *ferrotremolite* stability presented in this report are based on *rerun* synthetic assemblages consisting of high- and low-temperature equivalent assemblages. Phase relations were deduced by observing which assemblage grew at the expense of the other. In order to indicate the difficulties, sample X-ray diffractometer patterns of rather typicial low pressure, low temperature runs are presented in figure 3. As apparent from figure 3, proportions of the phases do not change markedly with time, at low pressures and temperatures. However, the ferrotremolite peaks are best developed and appear to be growing under P-T conditions interpreted as lying within the amphibole stability field; amphibole peaks decline and X-ray reflections for anhydrous phases increase in amplitude on experiments performed within the P-T field of the high-temperature phase assemblage.

Condensed run products were removed from the charge capsules, air dried at 110°C, and subsequently examined by means of (1) a 10 power hand lens, (2) a flat stage microscope using white light and refractive index oils of 0.002 refringence interval below 1.70, and 0.010 interval above 1.70 (mixed to 0.005), and (3) a Norelco X-ray diffractometer employing Fe$K\alpha$ radiation from 5-60°2θ. Synthetic quartz provided an internal diffraction

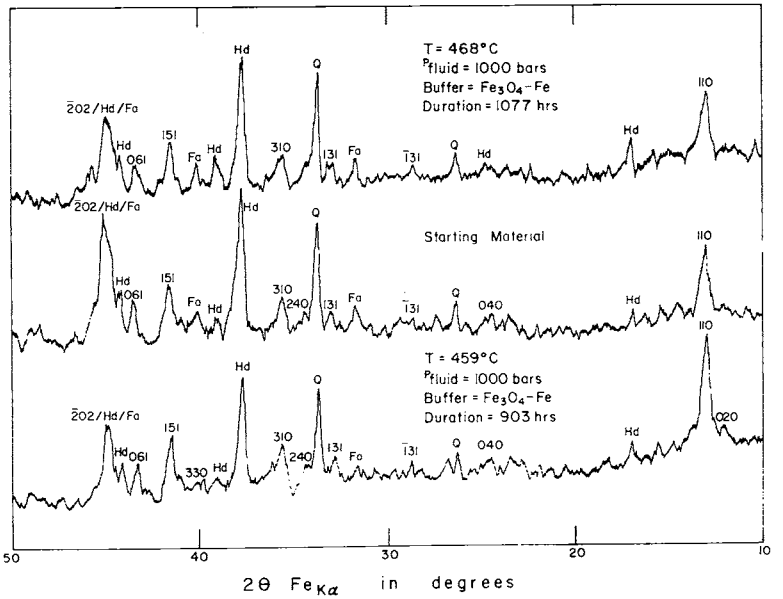

Fig. 3. Typical X-ray diffractograms illustrating method of curve location. The middle tracing represents starting material, upper and lower run products show growth of the high-temperature and low-temperature assemblages respectively (see also fig. 8). Hedenbergitic pyroxene and fayalite in particular exhibit well-defined reflections in the upper pattern, while ferrotremolite (indexed) peaks, especially 110, 310 and 151, are better developed in the lower pattern; quartz shows up well in all three diffractograms, but peak amplitudes are greatest in the upper and least in the lower.

standard for determinations of synthetic mineral unit cell dimensions (for method, see Ernst, 1962, p. 703).

DESCRIPTIONS OF SYNTHETIC PHASES

Ferrotremolite.—Ferrotremolite is stable only at low temperatures and relatively low oxygen fugacities roughly defined by the magnetite + quartz-fayalite and magnetite-iron buffers. Difficulty was experienced in converting the starting materials to 100 percent amphibole, although under given physical conditions, runs of longer duration produced more ferrotremolite than short runs. Moreover, where synthetic ferrotremolite-bearing assemblages were ground for one half hour in a mechanical grinder and then rerun, larger amounts of amphibole, up to approximately 95 volume percent of the charge, were crystallized (see table 7, run at T = 439°C, P_{fluid} = 3000 bars). The amphiboles produced in this study are thought to be "on composition", because phases of anhydrous condensed assemblages for the ferrotremolite bulk composition were present in the same relative proportions to one another, regardless of the amount of amphibole produced; optic and X-ray properties do not depend on the percentage of amphibole among run products. Mean indices of refraction and unit cell β angles (table 1) indicate that

the synthetic ferrotremolite does not represent solid solution with grunerite (see Deer, Howie, and Zussman, 1963, p. 234 and fig. 63).

Even on runs of very long duration, the amphibole produced consisted of pale yellow-green clots of exceedingly fine-grained needles and filaments randomly intergrown; individual crystals probably averaged about 0.3 x 0.3 x 5 microns, but such values are at the limit of resolution by microscopic methods. Mean indices of refraction on separate experiments range from 1.688 to 1.692 ± 0.003; optic data presented in table 1 show that this variation apparently is not systematically related to temperature, total fluid pressure, oxygen fugacity, or run duration.

Typical X-ray diffractometer patterns for synthetic ferrotremolite are presented in figure 3. The range of unit cell dimensions of ferrotremolite is: a = 9.95 — 9.98 ± 0.01Å, b = 18.31 — 18.39 ± 0.02Å, c = 5.28 — 5.32 ± 0.01Å, β = 104.3 — 104.7 ± 0.1°, and cell volume 937.5 — 941.4 ± 2.0Å^3. For comparison, optic and X-ray properties of a natural sample of manganous ferrotremolite, Tamarack-Custer mine, Coeur d'Alene district, Idaho (U.S. Natl. Mus. cat no. 93998, obtained through the courtesy of P. E. Desautels) is also shown in table 1. As suggested by the data presented in table 1 and in figure 4, only the b crystallographic axis of synthetic ferrotremolite seems to vary systematically with f_{O_2} and T: apparently b decreases slightly with increasing oxygen fugacity and diminishing temperature; how-

TABLE 1

Mean refractive index or NY and unit cell dimensions of synthetic and natural ferrotremolite

T, °C	P_{fluid}, bars	log f_{O_2}	run length, hrs	N mean	a, Å	b, Å	c, Å	β, °	cell v. Å^3
528	3000	—23.9	733	1.689	9.95	18.35	5.30	104.4	937.5
470	3000	—26.6	989	1.689	9.98	18.31	5.32	104.7	940.7
452	1000	—27.5	984	1.688	9.98	18.33	5.29	104.6	937.6
437	2980	—28.3	840	1.690	9.98	18.31	5.31	104.7	939.4
406	2000	—29.9	1604	1.691	9.98	18.32	5.32	104.7	941.4
537	3000	—27.6	475	1.688	9.97	18.39	5.28	104.4	938.1
516	3000	—28.5	602	1.689	9.98	18.35	5.30	104.6	939.0
503	2000	—29.1	820	1.690	9.96	18.36	5.30	104.3	938.7
459	1000	—31.4	903	1.688	9.97	18.35	5.30	104.5	937.7
420	500	—33.6	1125	1.691	9.97	18.34	5.30	104.5	937.5
synthetic ferrotremolite, avg				1.689	9.97	18.34	5.30	104.5	938.7
Mn-ferrotremolite (Shannon, 1921) *				1.682	9.96	18.32	5.30	104.6	936.7

Al	0.07	6 + 8 fold coordinated cations based on 24 anions
Fe+++	0.26	
Fe++	4.05	
Mn	0.47	
Mg	0.16	
total	5.01	

* Unit cell dimensions and NY determined by the present author.

ever, variation is almost within the limit of error of the X-ray measurements. This effect, if real, is tentatively attributed to increase in the $Fe^{+++}/_{Fe^{++}}$ ratio of ferrotremolite at elevated oxygen fugacities and low temperatures; inasmuch as the ionic radius of ferric iron, 0.64Å, is less than that of divalent iron, 0.74Å (Green, 1959), such mean valency increase and ionic radius decrease could account for a transverse octahedral strip contraction in the *b* axis direction. Zussman (1955) demonstrated that the sizes of the three octahedrally coordinated cation sites in actinolite are essentially identical; by analogy therefore, it is presumed that the minor Fe^{+++} in synthetic ferrotremolite is randomly distributed among these three sites. To maintain

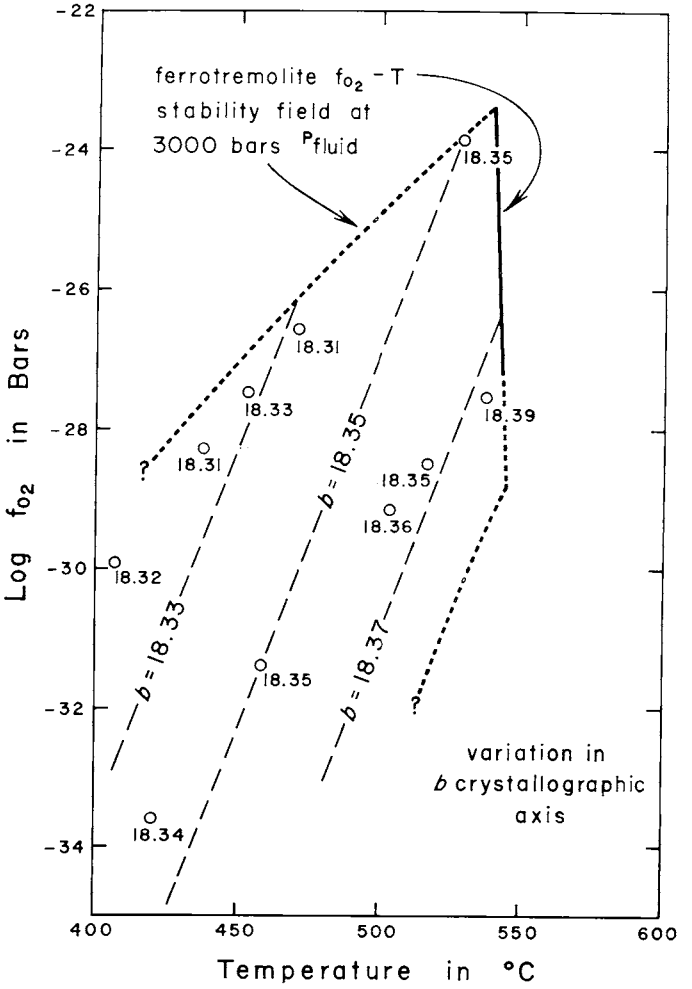

Fig. 4. Variation of ferrotremolite *b* crystallographic axis as a function of log f_{O_2} and T (data from table 1).

TABLE 2

NY of synthetic hedenbergite-ferrosilite solid solutions produced from $Hd_{100}Fs_{00}$, $Hd_{80}Fs_{20}$, and $Hd_{60}Fs_{40}$ bulk compositions, compared with natural hedenbergite

T, °C	P_{fluid}, bars	log f_{O_2}	run length, hrs	NY	mole proportion $FeSiO_3$ in pyroxene
724	2000	—19.9	113	1.731	0
611	2000	—24.1	167	1.728	0
720	2000	—20.0	113	1.738	20
603	2000	—24.5	167	1.734	20
715	2000	—20.2	113	1.744	40
608	2000	—24.3	167	1.740	40
hedenbergite (Muir, 1951, no. 19)				1.732	4

Al	0.145	6 + 8 fold coordinated cations based on 6 anions
Ti	0.037	
Fe+++	0.057	
Fe++	0.827	
Mn	0.025	
Mg	0.048	
Ca	0.761	
Na	0.048	
K	0.008	
total	1.956	

electrostatic neutrality, this process would require an equivalent replacement of OH by oxygen (oxyamphibole) as suggested for synthetic layer-lattice silicates (for example, see Eugster and Wones, 1962, p. 95-98; Wise and Eugster, 1964, p. 1051). The reaction involved is essentially $Fe^{++} + H^+$ (as hydroxyl) $= Fe^{+++} + \frac{1}{2} H_2$ (gas). Existence of hydroxyl-poor and hydroxyl-rich amphiboles has been demonstrated by Barnes (1930), Zussman (1955), and Hutton (1956).

Hedenbergitic pyroxene.—Clinopyroxene was produced in this study at temperatures in excess of the ferrotremolite stability field with f_{O_2} defined by the magnetite-iron, magnetite-wüstite, and magnetite + quartz-fayalite buffers; in addition, the pyroxene rather than ferrotremolite occurs at higher relative oxygen fugacity ranges with f_{O_2} controlled by the bunsenite-nickel buffer. Crystals are pale green, faintly pleochroic, blocky euhedra and range in average dimensions from 2 x 2 x 10 microns at low temperatures to about 10 x 10 x 20 microns near 700°C.

The optic properties and abundance of the pyroxene relative to other anhydrous phases appear to depend on the oxygen fugacity range. hence it was concluded that solid solutions intermediate between hedenbergite and ferrosilite might have been synthesized. Accordingly, the bulk compositions $CaFeSi_2O_6$ ($Hd_{100}Fs_0$), $Ca_{0.8}Fe_{1.2}Si_2O_6$ ($Hd_{80}Fs_{20}$), and $Ca_{0.6}Fe_{1.4}Si_2O_6$ ($Hd_{60}Fs_{40}$) were made up and crystallized to better than 98 percent homogeneous pyroxene under conditions where oxygen fugacities were controlled by

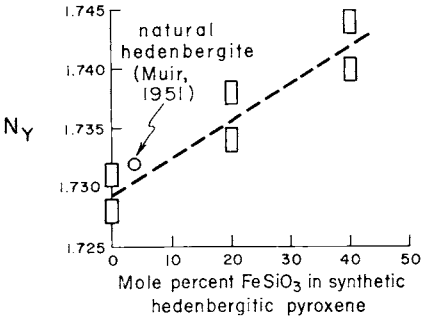

Fig. 5. Variation in N_Y for hedenbergitic members of the Hd-Fs solid solution series as a function of $FeSiO_3$ content (data from table 2). The determinative curve is only approximate.

the magnetite-wüstite buffer. Results are shown in table 2; a standard N_y versus composition curve is presented in figure 5. Refractive index differences as much as 0.004 were obtained for synthetic pyroxenes of presumably identical composition but grown under different experimental conditions. The discrepancies may represent measurement errors or may be a function of temperature of crystallization and/or run duration. Indices of refraction increase with increasing iron content of the pyroxene. Most natural members of the hedenbergite-ferrosilite series contain appreciable amounts of TiO_2, Fe_2O_3, and Na_2O and therefore display refractive indices greater than those of synthetic analogues produced in this study (for example, see Deer, Howie, and Zussman, 1963, table 7); however, a calcic pyroxene closely approaching the hedenbergite end member (Muir, 1961, tables II and III, no. 19) falls nearly on the synthetic pyroxene index-composition curve of figure 5.

Table 3 presents run data and N_y for pyroxenes crystallized from the ferrotremolite bulk composition under differing physical conditions. Compositions of the synthetic pyroxenes have been inferred from the standard curve presented in figure 5. Hedenbergitic limbs of two solvi are shown in figure 6, in which the data of table 3 are plotted. Equilibrium has not been demonstrated in these experiments, so figure 6 should be viewed with reservation. With f_{O_2} defined by a specific buffer, iron content of the pyroxene increases with elevated temperature. At a given temperature, more $FeSiO_3$ is incorporated in the pyroxene at low oxygen fugacity than at higher f_{O_2}. Data from experiments in which oxygen fugacities were defined by the magnetite-iron, magnetite-wüstite, and magnetite + quartz-fayalite buffers have been combined to give a single curve valid for a range of oxygen fugacities. For this range, the solvus is independent of oxygen fugacity inasmuch as the exsolution reaction, Fs-rich hedenbergite = Fs-poor hedenbergite + fayalite + quartz, does not evolve oxygen. On the other hand, the solvus for an oxidation state defined by the bunsenite-nickel buffer applies only to that *particular* f_{O_2} range, because oxygen takes part in the exsolution reaction, Fs-rich hedenbergite + oxygen = Fs-poor hedenbergite + magnetite + quartz.

With f_{O_2} defined by the magnetite-iron and magnetite-wüstite buffers, the synthetic pyroxene ranges from $Hd_{100}Fs_{00}$ near 400°C to $Hd_{60}Fs_{40}$ at about 625°C. Working at one atmosphere total pressure, Bowen, Schairer, and Posnjak (1933, p. 217-218) investigated this pyroxene series at a similarly low oxygen fugacity range but at higher temperatures; from N_x and N_z measurements they suggested that the maximum extent of iron solid solution at 850°C was 20 weight percent wollastonite-80 weight percent ferrosilite (= $Hd_{44}Fs_{56}$). In the present study, at a higher relative oxygen fugacity controlled by the bunsenite-nickel buffer, the pyroxene ranges from $Hd_{100}Fs_{00}$ near 400°C to $Hd_{80}Fs_{20}$ at approximately 625°C.

Bowen, Schairer, and Posnjak (1933) showed that Hd-Fs solid solutions invert to β-ferrowollastonite solid solutions at temperatures above 940 to 965°C. This transition has been corroborated by Yoder, Tilley, and Schairer (1963, p. 91). However, the present investigation was conducted at sufficiently low temperatures to prohibit the appearance of β-ferrowollastonite solid solutions.

TABLE 3

N_Y of synthetic hedenbergitic pyroxene produced from the ferrotremolite bulk composition

T, °C	P_{fluid}, bars	log f_{O_2}	run length, hrs	N_Y	mole proportion $FeSiO_3$ in pyroxene
611	500	—19.0	316	1.732	9
548	3000	—21.1	1176	1.731	6
540	3000	—21.4	1176	1.732	9
499	2000	—23.1	1511	1.729	0
487	2000	—23.6	1511	1.731	6
477	2000	—24.0	1511	1.729	0
440	3000	—25.8	2111	1.730	3
687	2000	—18.2	477	1.741	37
620	500	—20.4	316	1.741	37
571	3000	—22.2	696	1.739	30
558	3000	—22.7	696	1.736	21
535	3000	—23.6	2713	1.734	15
509	2000	—24.7	820	1.732	9
446	500	—27.8	903	1.729	0
682	2000	—21.4	477	1.743	43
610	500	—24.2	316	1.739	30
586	2995	—25.3	471	1.741	37
576	3000	—25.7	696	1.739	30
570	3000	—26.0	696	1.741	37
563	3000	—26.3	696	1.740	33
551	3010	—26.9	4877	1.737	24
478	1000	—30.3	1077	1.730	3
468	1000	—30.8	1077	1.729	0
450	500	—31.8	903	1.731	6

As demonstrated by Muir (1951), unit cell dimensions of naturally occurring hedenbergite-ferrosilites change only slightly as a function of composition. The d_{020} values were measured for synthetic standard pyroxene solid solutions and for 25 samples of pyroxene crystallized from the ferrotremolite bulk composition under various temperatures, fluid pressures, and oxygen fugacities. but *b* axis variation appears to lie within the ± 0.01Å limits of error of measurement.

Fayalite.—Fayalite is one of the phases produced by the high temperature decomposition of ferrotremolite in the oxygen fugacity range defined by the magnetite + quartz-fayalite, magnetite-wüstite, and magnetite-iron buffers. It occurs as very pale brown, minute, roughly equant subhedra, approximately one micron in diameter. Optic and X-ray data are presented in table 4. Within the limits of measurement these properties apparently are not affected by variation in temperature, P_{fluid}, f_{O_2}, and run duration. N_x averages 1.828 ± 0.003, in excellent agreement with the 1.827 value stated by Deer, Howie, and Zussman (1962, p. 2). The d_{130} was determined and averages 2.829 ± 0.001 Å, precisely the value reported by Yoder and Sahama (1957, table 2). Hence the olivine produced in this study seems to be pure fayalite and does not represent solid solution with kirschsteinite, the large-volume

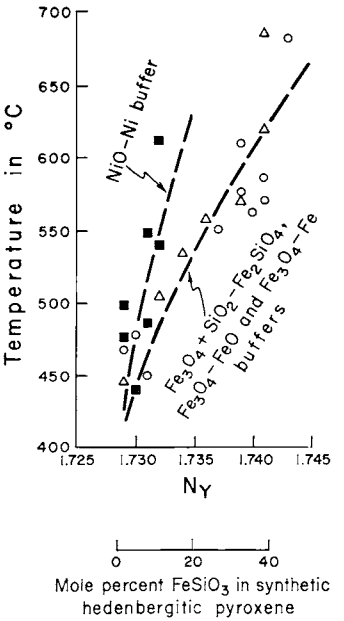

Fig. 6. Variation in N_Y for hedenbergitic pyroxene produced from the ferrotremolite bulk composition (data from table 3). Solid solution relations are inferred from the data of table 2, plotted graphically in figure 5, and are only tentative, because equilibrium has not been demonstrated. Oxygen fugacities defined by: magnetite-wüstite and magnetite-iron buffers = open circles; magnetite + quartz-fayalite buffer = open triangles; and bunsenite-nickel buffer = shaded boxes.

TABLE 4

Nx and d_{130} of synthetic fayalite compared to synthetic and natural olivine

T, °C	P_{fluid}, bars	log f_{O_2}	run length, hrs	Nx	d_{130}, Å
620	500	—20.3	316	1.827	2.828
611	500	—24.2	316	1,829	2,829
478	1000	—30.3	1077	1.827	2.829
natural fayalite, Deer, Howie, and Zussman (1962, p. 2)				1.827	
synthetic fayalite, Yoder and Sahama (1957, table 2)					2.829

calcium-iron analogue of monticellite (Sahama and Hytönen, 1957, give a d_{130} value of 2.9492Å for a natural sample of magnesian kirschsteinite).

Andradite.—Andradite was produced from the ferrotremolite bulk composition at high oxygen fugacities defined by the hematite-magnetite and hausmannite-manganosite buffers. It occurs as pale green equant euhedra of one to two microns diameter. Optic and X-ray data are presented in table 5. The index of refraction, 1.888 ± 0.003, is in excellent agreement with the value of 1.887 for synthetic andradite obtained by Skinner (1956, table 2). The measured *a*-axis length which averages 12.040 ± 0.010Å also compares well with Skinner's determination of 12.048Å. The data indicate that andradite produced in this investigation closely approaches the $Ca_3Fe_2^{+++}Si_3O_{12}$ end member and does not represent solid solution with hydrogarnet or with the hypothetical ferrous-ferric garnet, skiagite.

Hematite, magnetite, and quartz.—The phases hematite, magnetite, and quartz seem to exhibit inappreciable chemical variation under the investigated conditions so were examined in only cursory fashion. Mean grain sizes of these phases range from one to three microns. Hematite commonly grows as cherry red hexagonal platelets but only at high oxidation states defined by the hematite-magnetite and hausmannite-manganosite buffers. Magnetite generally forms clotted anhedra and was produced under conditions where oxidation state ranged from that defined by the magnetite + quartz-fayalite to the hematite-magnetite buffer. Quartz appears as a stable phase in all but hydrous mineral-bearing assemblages and generally occurs as anhedral grains; in

TABLE 5

Refractive index and unit cell edge of synthetic andradite

T, °C	P_{fluid}, bars	log f_{O_2}	run length, hrs	N	*a*, Å
620	500	—13.7	316	1.888	12.036
594	3010	—14.5	362	1.888	12.040
514	2990	—17.5	2423	1.889	12.040
513	1990	—18.2	2420	1.887	12.045
synthetic andradite, Skinner (1956, table 2)				1.887	12.048

some experiments, ditrigonal prisms terminated by presumably first and second order rhombohedra were observed.

Nontronite.—A montmorillonite-type phase was synthesized at low temperatures, high fluid pressures, and oxygen fugacities equal to or greater than those defined by the bunsenite-nickel buffer. This phase was not identified microscopically and must be exceedingly fine grained. This deduction is supported by the very poor X-ray diffraction patterns obtained. X-ray data are presented in table 6. The layer-lattice silicate produced is of the mixed-layer expandable montmorillonite-type as indicated by basal spacing collapse to about 12.6Å resulting from air drying at 110°C (comparable to values reported by Nagelschmidt, 1938, p. 148) and by basal spacing expansion to approximately 23.6Å on glycolization. Judging from the fact that it occurs in only moderate amounts and is associated with lime-bearing phases, the synthetic clay mineral contains very little calcium; its composition, provisionally considered as $Fe_2{+}{+}{+}Si_4O_{10}(OH)_2 \cdot n\,H_2O$, most closely approaches that of nontronite.

PHASE RELATIONS

Phase relations for the ferrotremolite bulk composition may be considered in terms of a five component system, Ca-Fe-Si-O-H. Oxygen contents of several of the phases are essentially univariant functions of temperature and oxygen fugacity inasmuch as total pressure appears to exert a negligible effect over the range of conditions investigated. All experiments were conducted with a small excess of H_2O over and above the amount necessary to saturate all phases in the component hydrogen (as OH or H_2O). Chemographic isothermal, isobaric relations are illustrated in figure 7 as a pseudoternary projection of condensed phase compositions along the hydrogen and

TABLE 6

X-ray data for synthetic clay mineral and natural nontronite

Natural nontronite Nagelschmidt (1938, p. 146)		Synthetic clay mineral					
		< 110°C		> 110°		after glycolization	
d in Å	I	d in Å	I	d in Å	I	d in Å	I
..	..	..	..	..	..	23.6	2
..	..	..	..	..	..	19.8	2
15.6	vs	15.9	3	12.6	10	15.9	2
..	..	8.0?	3	7.3	3	..	..
4.55	vs	4.53	2	4.39	2	4.42	3
..	..	4.18	1	4.08	1	..	..
..	..	..	..	3.78	1	3.86	1
3.11	vw	3.24	1	3.10	1	3.11	1
2.98	vw	..	..	3.01	1	3.02	1
2.62	s	2.61	1	..	..	2.61	1
2.56	s	2.55	1	2.57	1	..	..

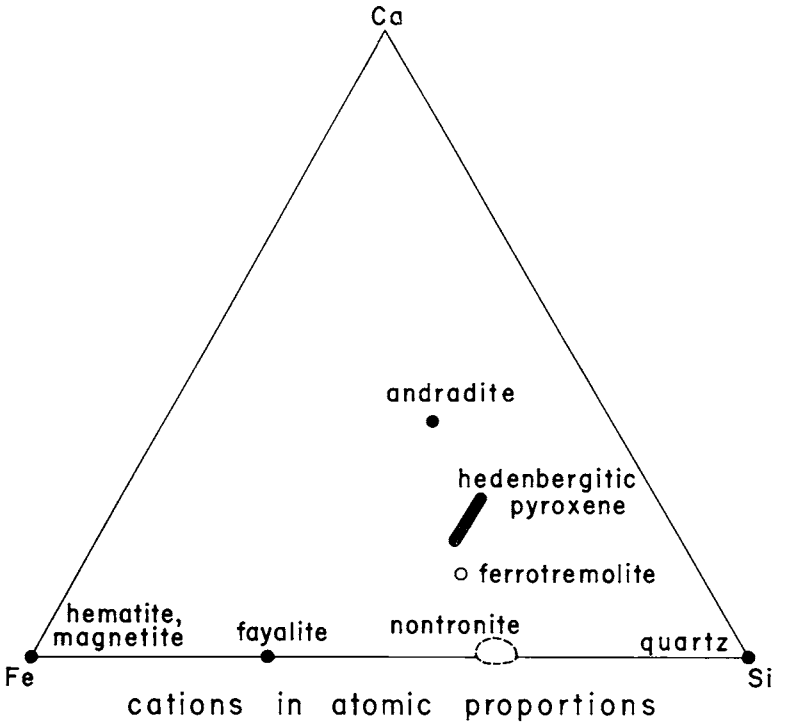

Fig. 7. Cation proportions for condensed phases produced from the ferrotremolite bulk composition under conditions of excess fluid ($\approx H_2O$), and variable oxygen content with f_{O_2} externally controlled by specific oxygen buffers.

oxygen axes onto the Ca-Fe-Si plane. Only phases produced in the study are shown in figure 7; grunerite and minnesotaite were not encountered under the investigated conditions.

P_{fluid}-T diagrams.—Conventional fluid pressure-temperature diagrams are presented in figures 8 to 10, with oxygen fugacities defined by the magnetite-wüstite and magnetite-iron, magnetite + quartz-fayalite, and bunsenite-nickel buffers respectively. Corresponding experimental run data are presented in tables 7 to 9. For investigations conducted employing the hausmannite manganosite buffer, hematite was prominent among the phases produced (see table 10), hence either the f_{O_2}-T curve extrapolated from the work of Hahn and Muan (1960) is incorrect, or H_2 equilibrium was not established between the buffer and charge capsules. The latter assumption is probably correct judging from the extremely low hydrogen fugacities in equilibrium with this buffer (hence negligible driving force for equilibrating buffer and charge). Accordingly, phase relations were not studied in detail using the hausmannite-manganosite buffer. Table 11 lists run data for experiments in which oxidation state was controlled by the hematite-magnetite buffer. Abbreviations used in the tables are as follows: And = andradite;

TABLE 7

Run data for the ferrotremolite bulk composition, f_{O_2} defined by the magnetite-wüstite and magnetite-iron buffers*

T, °C	P_{fluid}, bars	Duration, hrs	Condensed run products
398	490	1128	Ftr (+ Fa + Q + Hd)
409	490	1128	"
420	500	1125	"
437	540	4853	Ftr + Fa + Q + Hd
450	500	903	Fa + Q + Hd (+ Ftr)
610	500	316	Fa + Q + Hd
459	1000	903	Ftr (+ Fa + Q + Hd)
468	1000	1077	Fa + Q + Hd (+ Ftr)
478	1000	1077	"
421	2000	433	Ftr (+ Fa + Q + Hd)
493	2000	4495	"
503	2000	820	"
514	2000	820	Fa + Q + Hd
682	2000	477	"
429	3000	1102	Ftr (+ Fa + Q + Hd)
430	3000	383	"
439	3000	932	Ftr**
440	3000	1103	Ftr (+ Fa + Q + Hd)
446	3020	1098	"
456	3020	1098	"
470	3000	989	"
483	2990	983	"
489	3000	961	"
494	3005	624	"
503	3005	622	"
516	3000	602	"
537	3000	475	Ftr (+ Fa + Q + Hd)
551	3010	4877	Fa + Q + Hd (+ Ftr)
563	3000	696	"
570	3000	696	"
576	3000	696	"
586	2995	471	Fa + Q + Hd

* Starting material = Ftr + Fa + Q + Hd + H_2O; brackets denote metastable run products (that is, assemblage decreasing in amount).
** Traces of Fa + Q + Hd detectable by optic means only.

Fa = fayalite; Ftr = ferrotremolite; H = hematite; Hd = hedenbergitic pyroxene; Mt = magnetite; N = nontronite; and Q = quartz. Figures 8 to 10 exhibit the familiar P-T curves for thermal decomposition of hydrous phases; near the low oxygen fugacity limit of the magnetite f_{O_2}-T stability field, ferrotremolite was synthesized under equilibrium conditions, but at higher oxidation states where fayalite is unstable, the hydrous phase produced was nontronite. Melt was not encountered in the experimentally investigated P-T region.

Where oxygen fugacity is defined by the magnetite-wüstite and magnetite-iron buffers, ferrotremolite is stable below 543°C at 3000 bars fluid pressure (figure 8). The amphibole decomposes to a high-temperature assemblage of equivalent bulk composition consisting of the phases ferrosilite-rich heden-

bergitic pyroxene + fayalite + quartz + fluid. In a five component system, this field may be considered trivariant: independent variables are P_{fluid}, T, and f_{O_2}.

The heat of dehydration of ferrotremolite may be calculated employing the Clapeyron equation, $dP_{fluid}/dT = \Delta H/T\Delta V$, through measurement of the P_{fluid}-T curve slope, provided the volume change for the reaction can be obtained. The value of ΔH determined thus strongly depends on accurate measurement of dP_{fluid}/dT for the univariant curve, as pointed out by Orville and Greenwood (1965). Compositions and volumes of all solid phases participating in the reaction (some determined in this study) are known, assuming negligible ΔV contributions from thermal expansions and compressibility: these latter effects tend to cancel each other out anyway (for example, see Thompson, 1955, p. 68). Presuming the fluid phase to be nearly pure H_2O (see Kennedy, 1950; Holser and Kennedy, 1959), ΔV may

TABLE 8

Run data for the ferrotremolite bulk composition, f_{O_2} defined by the magnetite + quartz-fayalite buffer*

T, °C	P_{fluid}, bars	Duration, hrs	Condensed run products
397	500	458	Ftr (+ Mt + Fa + Q + Hd)
411	500	458	"
423	505	1009	"
424	530	4501	"
431	540	4853	Ftr + Mt + Fa + Q + Hd
442	540	4853	Mt + Fa + Q + Hd (+ Ftr)
446	500	903	"
620	500	316	Mt + Fa + Q + Hd
452	1000	984	Ftr (+ Mt + Fa + Q + Hd)
465	1000	930	Mt + Fa + Q + Hd (+ Ftr)
477	1000	930	"
494	1010	697	"
510	1010	697	"
406	2000	1604	Ftr (+ Mt + Fa + Q + Hd)
451	2000	433	"
498	2000	820	"
509	2000	820	Mt + Fa + Q + Hd (+ Ftr)
687	2000	477	Mt + Fa + Q + Hd
423	3000	2062	Ftr (+ Mt + Fa + Q + Hd)
432	3000	2062	"
437	2980	840	"
440	3000	1007	"
470	3000	989	"
523	3000	733	Ftr (+ Mt + Fa + Q + Hd)
528	3000	733	"
535	3000	2713	Ftr + Mt + Fa + Q + Hd
546	3010	4877	Mt + Fa + Q + Hd (+ Ftr)
558	3000	696	"
565	3000	696	"
571	3000	696	"

* Starting material = Ftr + Mt + Fa + Q + Hd + H_2O; brackets denote metastable run products (that is, assemblage decreasing in amount).

TABLE 9

Run data for the ferrotremolite bulk composition, f_{O_2} defined by the bunsenite-nickel buffer*

T, °C	P_{fluid}, bars	Duration, hrs	Condensed run products
349	520	2752	Ma + Q + Hd (+ Ftr)
356	520	2752	"
366	520	2752	"
373	520	2752	"
383	500	1728	"
390	500	1728	"
398	500	1728	"
406	500	1728	"
368	2000	1385	Mt + Hd + N (+ Ftr + Q)
377	2000	1385	Mt + Hd + N? (+ Ftr + Q)
395	2000	1071	Mt + Q + Hd (+ Ftr)
405	2000	1071	"
459	2000	433	"
477	2000	1511	"
487	2000	1511	"
499	2000	1511	"
548	2000	548	Mt + Q + Hd
353	3000	2922	Mt + Hd + N (+ Ftr)
401	3000	2924	"
414	3000	999	"
424	3000	999	"
440	3000	2111	Mt + Q + Hd (+ Ftr)
509	3010	957	"
521	3000	1176	Mt + Q + Hd
540	3000	1176	"
548	3000	1176	"

* Starting material = Ftr + Mt + Q + Hd + H_2O; brackets denote metastable run products (that is, assemblage decreasing in amount).

be computed for any temperature and pressure defined by the ferrotremolite dehydration curve. Calculated enthalpies at different curve sites with f_{O_2} controlled by the magnetite-iron buffer range from 6.8 to 7.9 ± 5 kcal/mole. The average of four values is 7.2 kcal/mole. This ΔH is comparable to enthalpies obtained by Taylor and Wells (1938) for the dehydration of coarse- and fine-grained brucite but is only 20 to 35 percent of the ΔH values determined by other workers for synthetic amphiboles and micas (for example, see compilation by Ernst, 1960, table 10).

At a higher relative oxygen fugacity range defined by the magnetite + quartz-fayalite buffer, ferrotremolite is stable up to a temperature of 539°C at 3000 bars fluid pressure (fig. 9). Magnetite joins the anhydrous assemblage of equivalent bulk composition. With five phases present, this high-temperature assemblage is divariant: at specified temperature and fluid pressure, oxygen fugacity and compositions of all the phases are uniquely defined. Computed heats of ferrotremolite dehydration with f_{O_2} defined by the magnetite + quartz-fayalite buffer range from 7.1 to 7.9 ± 5 kcal/mole. The aver-

TABLE 10

Run data for the ferrotremolite bulk composition, f_{O_2} defined by the hausmannite-manganosite buffer

T, °C	P_{fluid}, bars	Duration, hrs	Condensed run products
543*	1990	2420	And + H + Mt + Q
548**	1990	2420	"

* Starting material = And + H + Mt + Q + H_2O
** Starting material = Mt + Q + Hd + H_2O

age of four determinations is 7.5 kcal/mole. Similar enthalpy values for the dehydration compared to those obtained at a lower oxygen fugacity range (and similar dP/dT slopes) reflect approximately equal values of ΔV for the ferrotremolite breakdown reaction, inasmuch as a portion of the condensed assemblage of equivalent bulk composition, magnetite + quartz, has a volume comparable to that of fayalite + minor oxygen, except at very low pressures.

Under higher relative f_{O_2} ranges, the stability of ferrotremolite is severely restricted and gives way to an assemblage consisting of hedenbergitic pyroxene + magnetite + a ferric iron-bearing hydrous silicate, nontronite + fluid. Where f_{O_2} is defined by the bunsenite-nickel buffer, nontronite seems to be stable up to about 420°C at 3000 bars fluid pressure (fig. 10). It decomposes at higher temperatures apparently to magnetite + quartz (+ minor hedenbergitic pyroxene?) + fluid. It should be noted that nontronite grows from the ferrotremolite + magnetite + quartz + hedenbergitic pyroxene + fluid assemblage at temperatures at least at high as 414°C at 3000 bars P_{fluid}. Because of the extreme sluggishness of the reaction, the stable dehydration temperature of nontronite has not been determined. Hence, as shown in table

TABLE 11

Run data for the ferrotremolite bulk composition, f_{O_2} defined by the hematite-magnetite buffer*

T, °C	P_{fluid}, bars	Duration, hrs	Condensed run products
620	500	316	And + H + Mt + Q
426	2000	433	And + H + Mt + N? (+Q+Hd)
507	3000	1135	And + H + Mt + Q (+ Hd)
514	3000	136	"
514	2990	2423	And + H + Mt + Q
557	3010	362	"
594	3010	362	"

* Starting material = Ftr + Mt + Q + Hd + H_2O; brackets denote metastable run products (that is, assemblage decreasing in amount); ? = presence not definitely established.

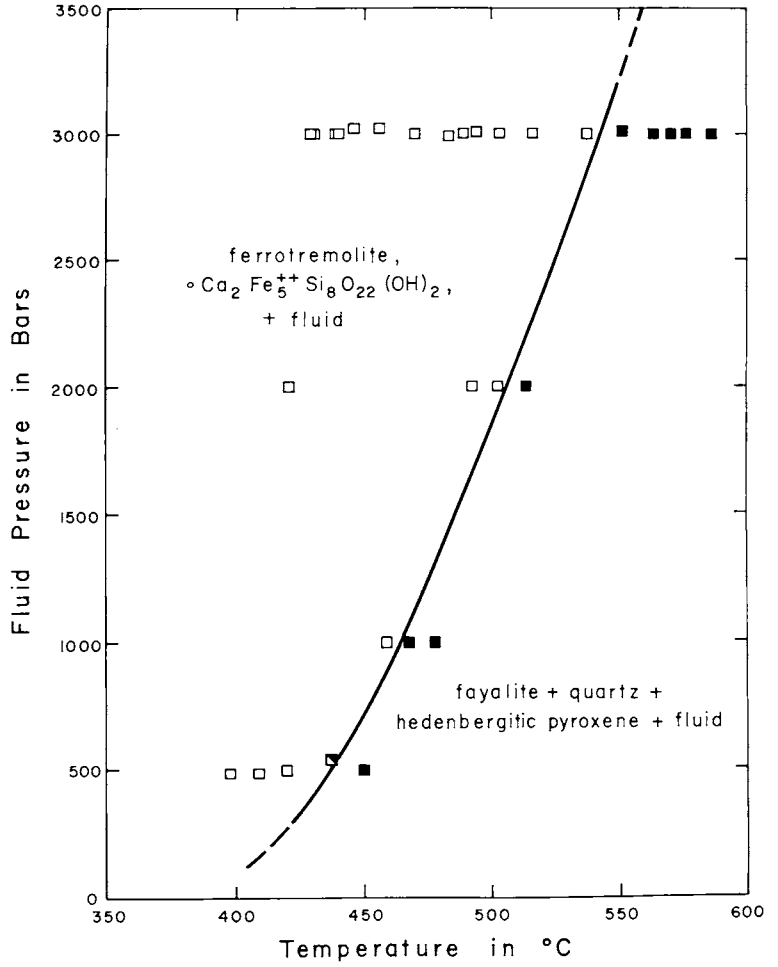

Fig. 8. P_{fluid}-T relations for the ferrotremolite bulk composition, with oxygen fugacities defined by the magnetite-wüstite and magnetite-iron buffers (data from table 7).

9, equilibrium has not been demonstrated adequately. Both high- and low-temperature assemblages are trivariant: temperature, fluid pressure, and either f_{O_2} or composition of the pyroxene solid solution may be considered as the three independent variables. In their studies of the system Fe-Si-O-H, neither Flaschen and Osborn (1957) nor Smith (1957) produced a montmorillonite-type mineral. These investigators worked principally at lower oxygen fugacity ranges, which could account for their failure to synthesize nontronite; on the other hand, small amounts of a large divalent cation—for instance, calcium in the present study—may be necessary to stabilize an iron-bearing clay mineral. Because of the large uncertainty as to the exact

composition of synthetic nontronite and P-T stability limit, it was not feasible to compute its heat of dehydration.

For more oxidizing conditions, with f_{O_2} defined by the hematite-magnetite buffer, nontronite probably decomposes above about 440°C at 3000 bars fluid pressure. For the ferrotremolite bulk composition, nontronite appears to be associated within its stability field with andradite + hematite + magnetite + fluid. As indicated in table 11, the experiments are insufficient and inconclusive; moreover, the starting material included hedenbergitic pyroxene, a phase metastable at such high oxygen fugacities. The high-temperature assemblage of equivalent bulk composition consists of the phases andradite +

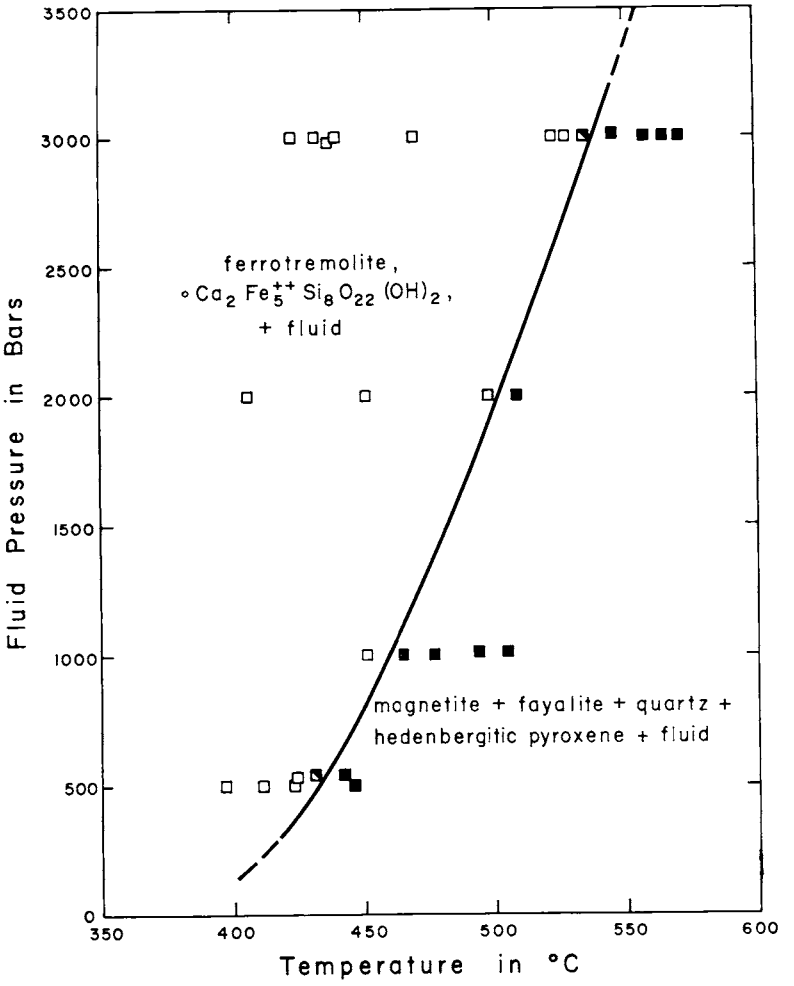

Fig. 9. P_{fluid}-T relations for the ferrotremolite bulk composition, with oxygen fugacities defined by the magnetite + quartz-fayalite buffer (data from table 8).

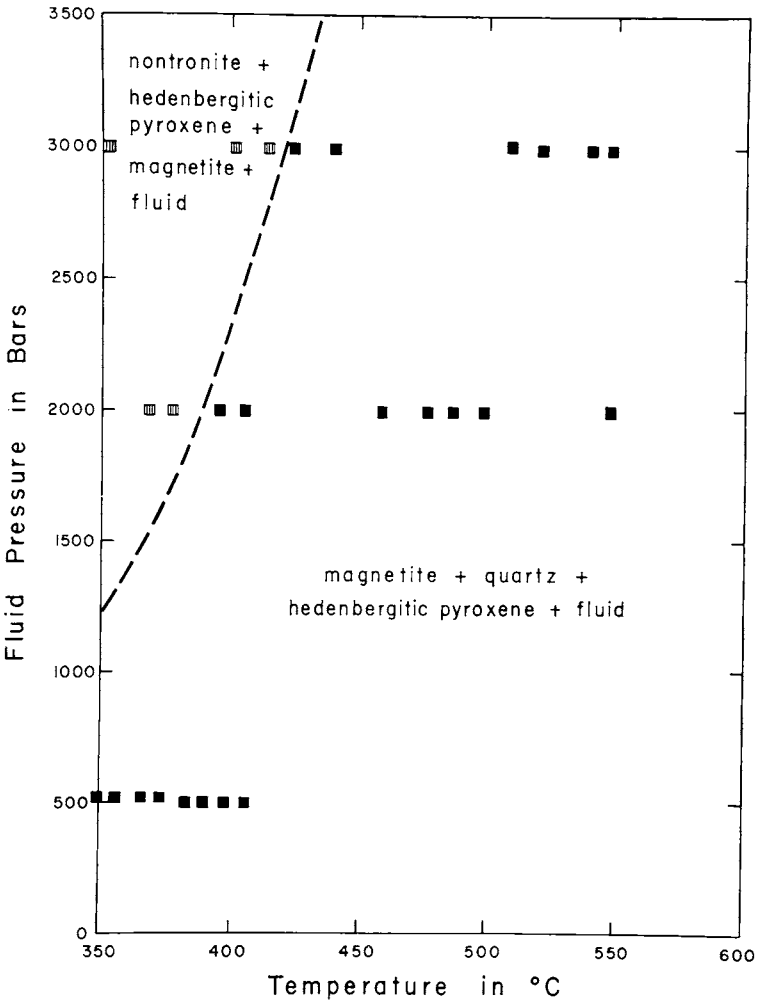

Fig. 10. P_{fluid}-T relations for the ferrotremolite bulk composition, with oxygen fugacities defined by the bunsenite-nickel buffer (data from table 9).

hematite + magnetite + quartz + fluid. In both high- and low-temperature fields there are two degrees of freedom, temperature and P_{fluid}; the assemblage itself uniquely specifies f_{O_2} and compositions of the phases.

f_{O_2}-T diagram.—The effect of oxygen fugacity at a constant fluid pressure of 3000 bars on the thermal ranges of the various assemblages is shown in figure 11. Field boundaries are presented as solid lines where experimentally verified in the present study or known from previous investigations of buffer assemblages in the system Fe-Si-O. Examples of the latter are curves (1), (4), and (8), the hematite-magnetite, magnetite + quartz-

fayalite, and fayalite-quartz + iron isobaric univariant equilibria respectively (see fig. 2). Dashed field boundaries are calculated or inferred.

The maximum thermal stability limit of ferrotremolite, figure 11, curve BCD, is essentially parallel to the oxygen fugacity ordinate because the dehydration of ferrotremolite to form fayalite + quartz + hedenbergitic pyroxene + fluid involves negligible amounts of oxygen. Actually, curve BCD should have a positive slope if O_2 were not involved in the dehydration reaction because at the low oxygen fugacity ranges defined by the magnetite-wüstite, magnetite-iron, and fayalite-iron + quartz buffers, f_{H_2} becomes appreciable and f_{H_2O} is correspondingly reduced (see Eugster and Wones,

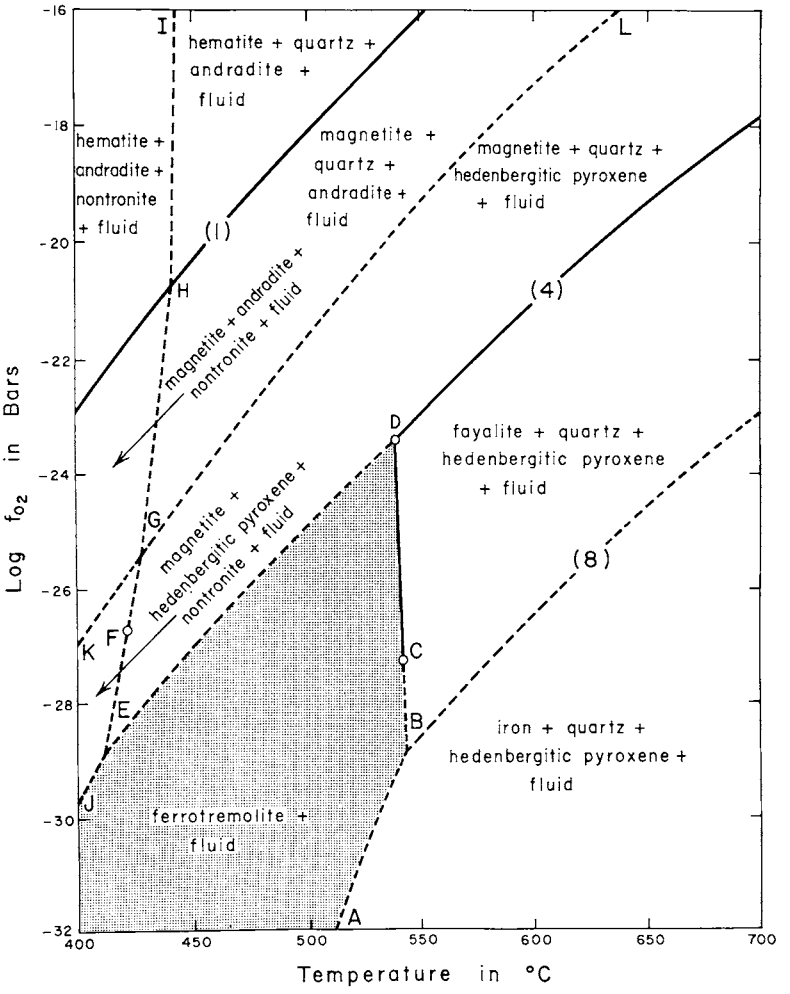

Fig. 11. f_{O_2}-T diagram at 3000 bars fluid pressure; field boundaries dashed where locations are calculated or inferred.

1962, fig. 3, also p. 115). The slightly negative log f_{O_2}/T slope for curve BCD suggests either that one or more condensed phases of the high-temperature assemblage contain minor amounts of ferric iron or that the amphibole might be more hydrogen-rich than assumed, especially in the lower oxygen fugacity region.

Pyroxene is presumed to be stable at lower oxygen fugacities than Fe_2SiO_4; if so, at low oxidation states defined by the fayalite-quartz + iron buffer, the high-temperature assemblage of equivalent bulk composition probably would consist of fayalite + quartz + iron + ferrosilite-rich hedenbergite + fluid. At constant temperature and even lower oxygen fugacities, this latter assemblage should be favored over ferrotremolite because of the low oxygen content of the condensed high temperature phases; the slope of the field boundary, figure 11, curve AB, cannot be computed because the pyroxene composition is not known precisely, but the log f_{O_2}-T slope must be positive inasmuch as the high-temperature assemblage is the large-volume assemblage (anhydrous reduced phases + O_2) with respect to ferrotremolite.

At oxidation states higher than that defined by the magnetite + quartz-fayalite buffer, the thermal range of ferrotremolite is severely restricted. The field boundary, figure 11, curve DE, has a positive slope because the low-temperature, relatively oxidized assemblage of magnetite + quartz + hedenbergitic pyroxene + fluid has a smaller volume than that of ferrotremolite + oxygen; hence increased f_{O_2} favors expansion of the more condensed, oxidized assemblage. The log f_{O_2}/T slope of this field boundary was approximated employing the Clausius-Clapeyron equation and a computed ΔH value for the reaction magnetite + quartz + hedenbergitic pyroxene + fluid = ferrotremolite + O_2 obtained through slope measurements (hence evaluation of ΔH) of the two experimentally determined curves specified by the reactions magnetite + quartz = fayalite + O_2 and ferrotremolite = fayalite + quartz + hedenbergitic pyroxene + fluid (for example, see Wones, ms). The computed curve lies just within the magnetite + quartz field of compatibility and nearly coincident with the f_{O_2}-T curve defined by the magnetite + quartz-fayalite buffer. Curve DE cannot be located accurately because of lack of detailed knowledge concerning compositions of the reacting phases, especially the fluid; nevertheless, computed relations must be *qualitatively* correct inasmuch as ferrotremolite is unstable at all oxygen fugacities defined by the bunsenite-nickel buffer (for example, point E must lie at a lower f_{O_2} than point F).

Nontronite-bearing assemblages are the most hydrous, oxidized assemblages produced, hence their high-temperature stability limits, figure 11, curves JE, EFG, GH, and HI, must be extended by increased f_{O_2}. Field boundaries could not be calculated because the exact composition of range of chemical variation of the clay mineral under the experimental conditions is unknown; therefore reactions could not be stated precisely.

Andradite appears in lieu of hedenbergitic pyroxene at high oxidation states, but neither the location nor f_{O_2}-T slope of the univariant reaction involving conversion of andradite + magnetite + quartz to hedenbergite +

oxygen, figure 11, curve KGL, could be determined because of insufficient calorimetric data and ignorance of the exact composition of the pyroxene. The sign of the f_{O_2}-T slope is positive inasmuch as the more oxidized, small-volume garnet-bearing assemblages are favored over hedenbergite + O_2 at elevated oxygen fugacities.

GEOLOGIC APPLICATION

As shown in figure 1, with the exception of manganous ferrotremolite occurring in amphibole + galena veins from the Coeur d'Alene district (Shannon, 1921) and actinolites from metamorphosed iron formations (for example, see Mueller, 1960, table 1), members of the $\square Ca_2Mg_5Si_8O_{22}(OH)_2$ $-\square Ca_2Fe_5{}^{++}Si_8O_{22}(OH)_2$ series closely approximate the compositions of

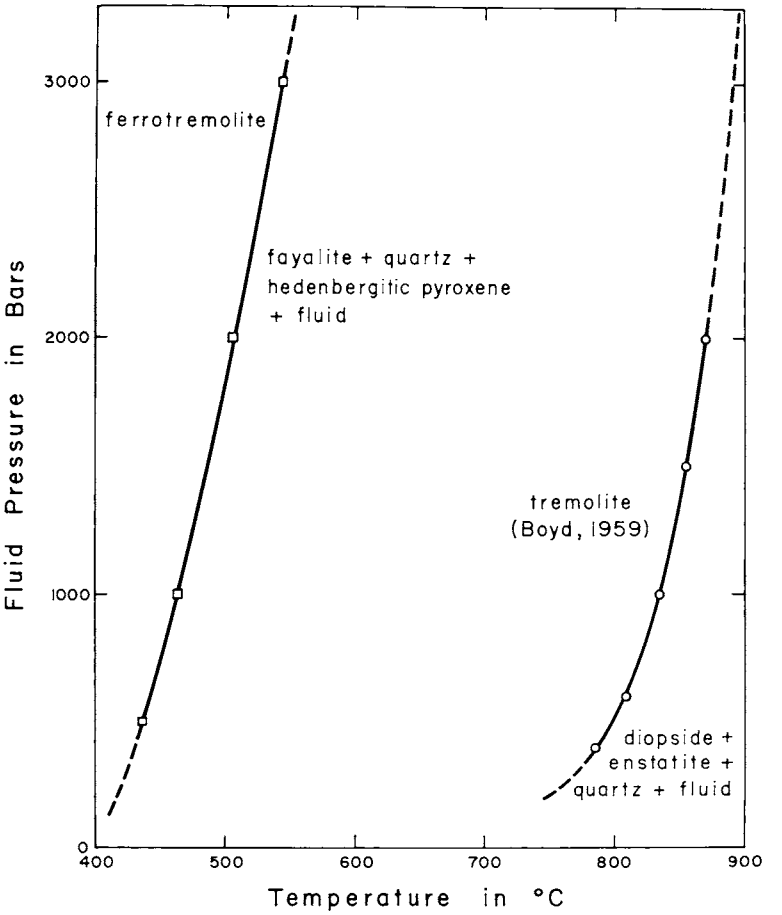

Fig. 12. Comparison of the high-temperature stability limits for tremolite (Boyd, 1959, fig. 3) and ferrotremolite (this study, fig. 8, f_{O_2} defined by magnetite-wüstite and magnetite-iron buffers).

tremolite and magnesian actinolite. This restriction to Mg-rich members of the series results from at least three different causes.

Firstly, tremolite has a greatly extended thermal stability range compared to the maximum high-temperature stability limit of ferrotremolite, as shown in figure 12. A rock having a bulk composition appropriately rich in CaO, FeO, SiO_2, and H_2O would contain ferrotremolite up to a definitely submagmatic temperature of only 543°C at 3000 bars fluid pressure; in contrast, tremolite would be stable up to approximately 890°C at 3000 bars P_{fluid} in a rock containing abundant CaO, MgO, SiO_2, and H_2O. A total ($=$ fluid $\approx$ H_2O) pressure of 3000 bars corresponds to a crystallization depth of 10 to 12 kilometers. Accordingly, at shallower depths, fluid pressures and consequently the thermal stability ranges of the amphiboles would be diminished. Moreover, if the equilibrium pressure of H_2O were less than total pressure (relatively low f_{H_2O}) stability of the hydrous minerals would be confined to lower temperatures (see discussions by Yoder, 1952: Thompson, 1955: Greenwood, 1961; and Barnes and Ernst, 1963) compared to conditions where P_{H_2O} is equivalent to lithostatic pressure.

Secondly, because it contains iron predominantly as the ferrous ion, oxygen fugacities in excess of those defined by the assemblage magnetite + quartz-fayalite cause a drastic reduction in the stability range of ferrotremolite as demonstrated by the experimental study (fig. 11). Practically all metamorphic rocks crystallize at oxygen fugacities within the magnetite f_{O_2}-T stability field (Eugster, 1959). Graphitic schists (Miyashiro, 1964) and marbles (Mueller and Condie, 1964) apparently formed under relatively low oxygen fugacities, but such bulk compositions are inappropriate for the production of ferrotremolite. Many glaucophane schists and greenschists crystallized under relatively oxidizing conditions (for example, see Banno and Kanehira, 1961; Ernst, 1962, p. 734; Iwasaki, 1963, p. 32-34); hence in these cases metamorphism failed to develop an iron-rich calcic amphibole because of relatively high f_{O_2}.

Thirdly, although some sandy dolomitic marbles rather closely approximate the bulk composition of tremolite, most rocks deviate markedly from that of ferrotremolite in that high CaO and FeO are seldom associated in the near absence of MgO and Al_2O_3. Thus, with a single exception of a peculiar vein filling occurrence, the $\square Ca_2Fe_5^{++}Si_8O_{22}(OH)_2$ end member has not been reported as a natural mineral. Intermediate members of the tremolite-ferrotremolite series are predominately Mg-rich. Actinolites of roughly subequal Mg-Fe^{++} proportions are restricted to metamorphosed iron formations low in alumina. Because the partitioning of iron and magnesium among ferromagnesian silicates tends to enrich the more refractory anhydrous phases in iron, coexistent actinolites are relatively enriched in Mg. Such relations are illustrated in figure 13, a schematic isothermal, isobaric section through the SiO_2+H_2O saturated system CaO-MgO-FeO. Physical conditions presumed are such that iron-rich actinolites, cummingtonites, and layer-lattice silicates are not stable. Phase equilibrium relations involving the latter two mineral groups are unknown, hence they have not been considered in figure 13. How-

ever, actinolite + grunerite and fayalite + hypersthene + cummingtonite + hedenbergite assemblages have been reported by Mueller (1960) and Gunderson and Schwartz (1962, p. 85) respectively. Judging from descriptions by Gunderson and Schwartz (1962, p. 97-100), minnesotaite, nontronite, and stilpnomelane are very low-grade or retrograde metamorphic minerals. Tie lines from experimental work (Bowen and Schairer, 1935) and natural mineral assemblages (Mueller, 1960) were utilized in figure 13 insofar as possible, but precise slopes are not necessarily reproduced: slopes of tie lines between coexisting cummingtonites and actinolites indicate that the iron : magnesium ratio in cummingtonite is higher than it is in actinolite. similar to the hypersthene-actinolite equilibria depicted schematically. The point of importance is that iron-rich bulk compositions will carry actinolite relatively enriched in magnesium or none at all.

In summary, the experimental investigation has demonstrated that the rarity of ferrotremolite results from its relatively low thermal stability range, its restriction to very low relative oxygen fugacity ranges, and to departure of rock bulk compositions from that of $Ca_2Fe_5^{++}Si_8O_{22}(OH)_2$. Such an amphibole can exist however. and future investigations (for instance, electron

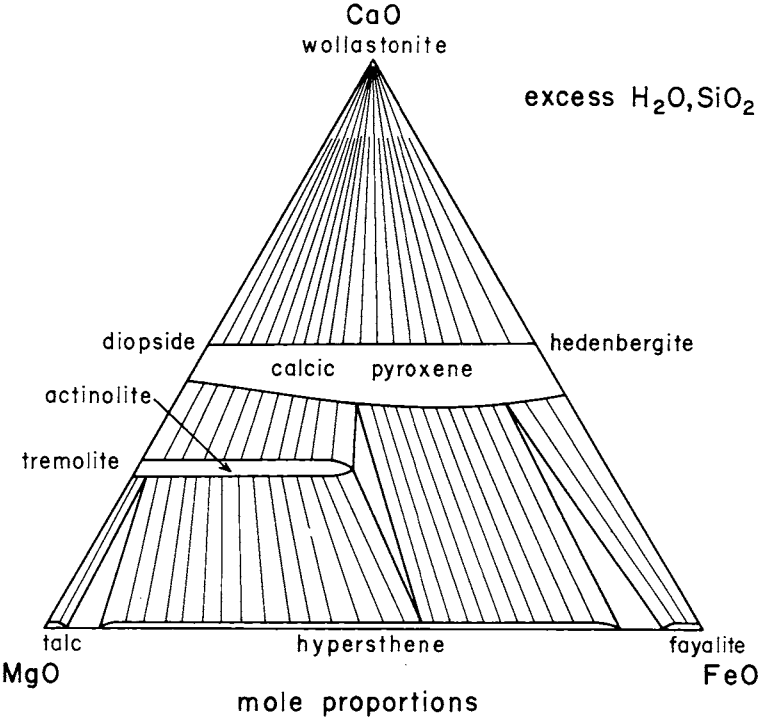

Fig. 13. Diagrammatic isothermal, isobaric section of the SiO_2 + H_2O saturated system CaO-MgO-FeO. Phase relations involving iron-rich layer-lattice silicates and grunerite have not been considered (see text for discussion).

microprobe studies of amphiboles from meta iron formations, and of iron-rich uralites from igneous rocks) may indicate that ferrotremolite is more common than presently suspected.

References

Banno, Shohei, and Kanehira, Keiichiro, 1961, Sulfide and oxide minerals in schists of the Sanbagawa and central Abukuma metamorphic terranes: Japanese Jour. Geology and Geography, v. 32, p. 331-348.

Barnes, H. L., and Ernst, W. G., 1963, Ideality and ionization in hydrothermal fluids: the system MgO-H_2O-$NaOH$: Am. Jour. Sci., v. 261, p. 129-150.

Barnes, V. E., 1930, Changes in hornblende at about 800°C: Am. Mineralogist, v. 15, p. 393-417.

Berman, Harry, 1937, Constitution and classification of the natural silicates: Am. Mineralogist, v. 22, p. 342-408.

Bowen, N. L., Schairer, J. F., and Posnjak, Eugen, 1933, The system, CaO-FeO-SiO_2: Am. Jour. Sci., 5th ser., v. 26. p. 193-284.

Bowen, N. L., and Schairer, J F, 1935, The system MgO-FeO-SiO_2: Am. Jour. Sci., 5th ser., v. 29, p. 151-217.

Boyd, F. R., 1959, Hydrothermal investigations of amphiboles, *in* Abelson, P. H., ed., Researches in geochemistry: New York, John Wiley and Sons, Inc., p. 377-396.

Deer, W. A., Howie, R. A., and Zussman, J., 1962, Rock-forming minerals. Vol. 1. Ortho- and Ring Silicates: New York, John Wiley and Sons, Inc., 333 p.

———— 1963, Rock-forming minerals. Vol. 2, Chain Silicates: New York, John Wiley and Sons, Inc., 379 p.

Ernst, W. G., 1960, The stability relations of magnesioriebeckite: Geochim. et Cosmoch. Acta, v. 19, p. 10-40.

———— 1962, Synthesis, stability relations, and occurrence of riebeckite and riebeckite-arfvedsonite solid solutions: Jour. Geology, v. 70, p. 689-736.

Eugster, H. P., 1957, Heterogeneous reactions involving oxidation and reduction at high pressures and temperatures: Jour. Chem. Physics, v. 26, p. 1760-1761.

———— 1959, Reduction and oxidation in metamorphism, *in* Abelson, P. H., ed., Researches in geochemistry: New York, John Wiley and Sons, Inc., p. 397-426.

Eugster, H. P., and Wones, D. R., 1962, Stability relations of the ferruginous biotite, annite: Jour. Petrology, v. 3, p. 82-125.

Flaschen, S. S., and Osborn, E. F., 1957, Studies of the system iron oxide-silica-water at low oxygen partial pressures: Econ. Geology, v. 52, p. 923-943.

Gilbert, M. C., 1965, Synthesis and stability relationships of the hornblende, ferropargasite [abs.]: Geol. Soc. America Spec. Paper 82, p. 72-73.

Green, Jack, 1959, Geochemical table of the elements for 1959: Geol. Soc. America Bull., v. 70, p. 1127-1184.

Greenwood, H. J., 1961, The system $NaAlSi_2O_6$-H_2O-Argon: total pressure and water pressure in metamorphism: Jour. Geophys. Research, v. 66, p. 3923-3946.

Gunderson, J. N., and Schwartz, G. M., 1962, The geology of the metamorphosed Biwabik iron-formation, Eastern Mesabi District, Minnesota: Minn. Geol. Survey Bull. 43, 139 p.

Hahn, W. C. Jr., and Muan, Arnulf, 1960, Studies in the system Mn-O: the Mn_2O_3-Mn_3O_4-MnO equilibria: Am. Jour. Sci., v. 258, p. 66-78.

Hallimond, A. F., 1943, On the graphical representation of the calciferous amphiboles: Am. Mineralogist, v. 28, p. 65-89.

Holser, W. T., and Kennedy, G. C., 1959, Properties of water. Pt V. Pressure-volume-temperature relations of water in the range 400-1000C and 100-1400 bars: Am. Jour. Sci., v. 257, p. 71-77.

Hutton, C. O., 1956, The composition of an actinolite: Acta Cryst., v. 9, p. 231-232.

Iwasaki, M., 1963, Metamorphic rocks of the Kôtu-Bizan area, eastern Sikoku: Tokyo Univ., Fac. Sci. Jour., sec. II, v. 15, p. 1-90.

Kennedy, G C., 1950, Pressure-volume-temperature relations in water at elevated temperatures and pressures: Am. Jour. Sci., v. 248, p. 540-564.

Kunitz, W., 1930, Die Isomorphieverhaeltnisse in der Hornblendegruppe: Neues Jahrb. Mineralogie, Beil. Bd. 60, A, p. 171-250.

Leake, B. E., 1965, The relationship between tetrahedral aluminum and the maximum possible octahedral aluminum in natural calciferous and subcalciferous amphiboles: Am. Mineralogist, v. 50, p. 843-851.

Miyashiro, A., 1964, Oxidation and reduction in the Earth's crust with special reference to the role of graphite: Geochim et Cosmochim. Acta, v. 28, p. 717-729.

Mueller, R. F., 1960, Compositional characteristics and equilibrium relations in mineral assemblages of a metamorphosed iron formation: Am. Jour. Sci., v. 258, p. 449-497.

Mueller, R. F., and Condie, K. C., 1964, Stability relations of carbon mineral assemblages in the Southern California Batholith: Jour. Geology, v. 72, p. 400-411.

Muir, I. D., 1951, The clinopyroxenes of the Skaergaard intrusion, eastern Greenland: Mineralog. Mag., v. 29, p. 690-714.

Nagelschmidt, G., 1938, On the atomic arrangement and variability of the members of the montmorillonite group: Mineralog. Mag., v. 25, p. 140-155.

Orville, P. M., and Greenwood, H. J., 1965, Determination of ΔH of reaction from experimental pressure-temperature curves: Am. Jour. Sci., v. 263, p. 678-683.

Sahama, Th.G., and Hytönen, K., 1957, Kirschsteinite, a natural analogue to synthetic iron monticellite, from the Belgian Congo: Mineralog. Mag., v. 31, p. 698-699.

Shannon, E. V., 1921, Description of ferroanthophyllite, an orthorhombic iron amphibole from Idaho, with a note on the nomenclature of the anthophyllite group: U.S. Natl. Mus. Proc., v. 59, p. 397-401.

Skinner, B. J., 1956, Physical properties of end-members of the garnet group: Am. Mineralogist, v. 41, p. 428-436.

Smith, J. R., 1957, Reconnaissance in the system FeO-Fe_2O_3-SiO_2-H_2O: Carnegie Inst. Washington Year Book 56, p. 230-231.

Sundius, N. G., 1946, The classification of the hornblendes and the solid solution relations in the amphibole group: Sveriges Geol. Undersökning, Årsbok 40, no. 4, 36 p.

Taylor, K., and Wells, L., 1938, Studies of the heat of solution of calcium and magnesium oxides and hydroxides: U.S. Natl. Bur. Standards, Jour. Research, v. 21, p. 133-149.

Thompson, J. B, Jr., 1955, The thermodynamic basis for the mineral facies concept: Am. Jour. Sci., v. 253, p. 65-103.

Tuttle, O. F., 1949, Two pressure vessels for silicate-water studies: Geol. Soc. America Bull., v. 60, p. 1727-1729.

Warren, B. E., 1929, The structure of tremolite: Zeitschr. Kristallographie, v. 72, p. 42-57.

———— 1930, The crystal structure and chemical composition of the monoclinic amphiboles: Zeitschr. Kristallographie, v. 72, p. 493-517.

Winchell, A. N., and Winchell, Horace, 1951, Elements of optical mineralogy: New York, John Wiley and Sons, Inc., 551 p.

Wise, W. S., and Eugster, H. P., 1964, Celadonite: synthesis, thermal stability and occurrence: Am. Mineralogist, v. 49, p. 1031-1083.

Wones, D. R., ms, 1960, Phase relations of the biotites: Ph.D. thesis, Mass. Inst. Technology, Cambridge, Mass.

Yoder, H. S., Jr., 1952, The MgO-Al_2O_3-SiO_2-H_2O system and the related metamorphic facies: Am. Jour. Sci., Bowen v., p. 569-627.

Yoder, H. S., Jr., and Sahama, Th.G., 1957, Olivine X-ray determinative curve: Am. Mineralogist, v. 42, p. 475-491.

Yoder, H. S., Jr., Tilley, C. E., and Schairer, J. F., 1963, Pyroxenes and associated minerals in the crust and mantle: Carnegie Inst. Washington Year Book 62, p. 84-95.

Zussman, J., 1955, The crystal structure of actinolite: Acta Cryst., v. 8, p. 301-308.